Translational Oncology
www.transonc.com

Volume 11 Number 3 June 2018 pp. 599–608 599

Concurrent Treatment with Anti-DLL4 Enhances Antitumor and Proapoptotic Efficacy of a γ-Secretase Inhibitor in Gastric Cancer[1,2]

Muxing Kang[*,†], Yaoyi Zhang[*], Xiaoli Jin[*], Guofeng Chen[*], Yi Huang[*], Dan Wu[*], Guogang Li[*], Jianzhen Shan[‡], Pintong Huang[§] and Jian Chen[*]

[*]Department of Surgery, Second Affiliated Hospital, Zhejiang University School of Medicine, Hangzhou, Zhejiang, 310000, China; [†]Key Laboratory of Cancer Prevention and Intervention, China National Ministry of Education, Cancer Institute, Second Affiliated Hospital, Zhejiang University School of Medicine, Hangzhou, Zhejiang, 310000, China; [‡]Department of Oncology, Second Affiliated Hospital, Zhejiang University School of Medicine, Hangzhou, Zhejiang, 310000, China; [§]Department of Radiology, Second Affiliated Hospital, Zhejiang University School of Medicine, Hangzhou, Zhejiang, 310000, China

Abstract

The Notch signaling pathway has been identified as a therapeutic target for cancers. γ-Secretase inhibitors (GSIs) have been progressively recognized as potential anticancer drugs. The present study aimed to investigate the effects of anti-delta like legend 4 (anti-DLL4) treatment on the anticancer efficacy of GSIs in gastric cancer. SGC-7901-GFP human gastric cancer cells were tested for DLL4 expression by rosette formation test and immunofluorescence, and then were treated with anti-DLL4 antibody N-[N-(3,5-difluorophenacetyl)-L-ananyl]-S-phenylglycine t-butyl ester (DAPT, a type of GSI), or a combination of anti-DLL4 antibody and DAPT. The effects of *in vitro* treatments on cell apoptosis, cell cycle, and cell invasion were analyzed. For *in vivo* study, an orthotopic mouse model of gastric cancer was established with green fluorescence expressing SGC-7901. Ultrasound targeted microbubble destruction was used to treat tumor-bearing mice with anti-DLL4 antibody conjugated microbubbles, DAPT, and a combination of the two. Real-time fluorescence imaging was performed to assess tumor cell inhibition in each group. Following *in vivo* treatments, apoptosis of tumor cells and the expression of apoptosis-related genes BAX, Bcl-2, and P53 were detected by TUNEL and immunohistochemical staining. *In vivo* combined treatment of anti-DLL4 and DAPT led to a higher rate of cell apoptosis and greater inhibition of cell invasion than that observed with DAPT treatment alone. DAPT and anti-DLL4 combination therapy resulted in decreased cell distribution at G1 phase and increased cell distribution at S phase, compared to the untreated control group ($P < .01$). *In vivo* combined therapy with anti-DLL4 and DAPT significantly increased tumor growth inhibition and tumor cell apoptosis when compared to DAPT therapy alone ($P < .05$). In addition, combined treatment significantly increased expression of BAX and P53 and reduced Bcl-2 expression ($P < .05$). Conversely, treatment with DAPT alone only increased expression of BAX and P53 ($P < .05$), suggesting that the reduction of Bcl-2 expression may play an important role in the synergetic antitumor and proapoptosis effects of the combined treatment. Concurrent treatment with anti-DLL4 enhances the antitumor and proapoptotic efficacy of the γ-secretase inhibitor in gastric cancer both *in vitro* and *in vivo*.

Translational Oncology (2018) 11, 599–608

Address all correspondence to: Jian Chen, MD & PhD, Department of Surgery, Second Affiliated Hospital, Zhejiang University School of Medicine, 88 Jiefang Road, Hangzhou, 310009, China. E-mail: zrchenjian@zju.edu.cn or Pintong Huang, MD & PhD, Department of Radiology, Second Affiliated Hospital, Zhejiang University School of Medicine, 88 Jiefang Road, Hangzhou, 310009, China. E-mail: huangpintong@126.com

[1] Conflict of Interest: We declare that there was no conflict of interest.

[2] Acknowledgements: Dr. Jian Chen was supported by the National Natural Science Foundation of China (no. 81372620 and 81271584) and Natural Science Foundation of Zhejiang Province (no. LY14H160034). Dr. Muxing Kang was supported by the National Natural Science Foundation of China (no. 81301889). Dr. Pintong Huang was supported by the National Natural Science Foundation of China (no. 81420108018 and 81527803).

Received 13 November 2017; Revised 14 February 2018; Accepted 19 February 2018

1936-5233/18
https://doi.org/10.1016/j.tranon.2018.02.016

Introduction

Gastric cancer (GC) is the fifth most common malignancy and the second leading cause of cancer death in the world [1]. Although radical resection is the optimal treatment for GC, only a quarter of these patients are diagnosed in the early stages of the condition, and the overall survival for the majority of patients with GC is dismal [2]. Medications currently used in the treatment of GC have a low success rate, and patients develop rapid tolerance to these drugs [3]. Therefore, there is a dire need for new treatment regimens for GC patients.

The Notch signaling pathway has been identified as a therapeutic target for cancers. It is known to regulate a number of cellular processes, including cell proliferation, apoptosis, migration, invasion, and angiogenesis [4–7]. The Notch genes encode proteins that are activated by interacting with a family of ligands. Upon activation, Notch is cleaved, releasing the intracellular domain part of Notch (ICN), which goes through a cascade of proteolytic cleavages by the metalloprotease, tumor necrosis factor-α converting enzyme, and the γ-secretase complex [8,9]. Delta-like ligand 4 (DLL4) is involved in the Notch signaling pathway as a ligand for Notch1 and Notch4 [7,10,11]. Studies have indicated that the DLL4-Notch system plays a critical role in tumor neovascularization and metastasis in some malignancies [12–14]. DLL4 is highly expressed in several human cancers [15,16]. Several preclinical xenograft studies have demonstrated that DLL4 blockade results in ineffective angiogenesis, promotion of apoptosis, inhibition bulk tumor cells, and reduced tumorigenic cells or cancer stem cell proliferation [17–19]. Moreover, γ-secretase inhibitors (GSIs) have been progressively recognized as potential anti-cancer drugs [20].

N-[N-(3,5-difluorophenacetyl)-L-ananyl]-S-phenylglycine t-butyl ester (DAPT), a type of GSI, is widely used to inhibit Notch activation. It has been reported that DAPT inhibits growth, invasion, and metastasis of some cancer cells [21]. However, the therapeutic effect of anti-DLL4 and GSIs on GC remains unclear. Our previous report indicated that DLL4 upregulation in gastric cancer cells promoted cell proliferation, migration, *in vitro* invasion, and *in vivo* tumorigenesis [22]. Therefore, the present study aimed to investigate the effects of DLL4 blockade on GSI-mediated anticancer activity in gastric cancer through the ultrasound targeted microbubble destruction (UTMD) to deliver anti-DLL4 and DAPT for therapy in orthotopic gastric cancer mouse models. The findings of this study suggest a synergetic antitumor effect of combined anti-DLL4 and DAPT therapy in GC.

Materials and Methods

Cell Culture

Human gastric cancer cell line (SGC-7901-GFP) expressing green fluorescent protein (GFP) was obtained from AntiCancer, Inc. (San Diego, CA). Cells were cultured in an RPMI 1640 medium (Thermo Fisher Scientific, CA) containing 10% fetal bovine serum (Thermo Fisher Scientific, CA), 100 U/ml penicillin, and 100 μg/ml streptomycin (Thermo Fisher Scientific, CA) at a temperature of 37°C with 5% CO_2.

Preparation of Targeted Microbubbles

Targestar-SA microbubbles (MB, Targeson Inc., San Diego, CA) were used for the UTMD technique. Targestar-SA is an ultrasound contrast agent composed of a perfluorocarbon gas core encapsulated in a lipid shell. The outer shell is derivatized with streptavidin, which binds biotinylated ligands at a density of 80 to 220 × 10^3 molecules per microbubble. The agent has a median diameter of approximately 2.0 μm. Microbubbles were incubated with biotinylated anti-DLL4 antibody (BIOLEGEND) at room temperature for 20 minutes at a ratio of 0.7 nmol of the antibody per 10^9 microbubbles. The unreacted antibodies were removed from the microbubbles by centrifugal washing according to the manufacturer's recommended protocol. Quantitation of microbubble-bound anti-DLL4 antibody was done by BCA Protein Assay (Pierce, Rockford, IL), which revealed a maximum antibody payload of 9.7 μg per 10^9 microbubbles. Unconjugated Targestar-SA microbubbles were used directly from the vial without the addition of ligands.

Rosette Formation Test

Expression of DLL4 on the SGC-7901-GFP cell was verified by the rosette formation test. The cultured SGC-7901-GFP cell line was collected and divided into three groups. The cells in group 1 were added to unconjugated microbubbles and served as the negative control. The cells in group 2 were added to anti-DLL4 antibody conjugated microbubbles, and the cells in group 3 were first blocked by the anti-DLL4 antibody and then incubated with anti-DLL4 antibody conjugated microbubbles. Following an incubation period of 30 minutes at room temperature, images of the cells in each group were captured using an upright metallurgical microscope (Olympus BX53, Tokyo, Japan).

Immunofluorescence Staining

Expression of DLL4 on the SGC-7901-GFP cell was further confirmed by immunofluorescence. A total of 1 × 10^5 SGC-7901-GFP cells were plated on coverslips placed in 6-well plates. After leaving the cells to adhere to the dish for 1 day, the cells were washed with phosphate-buffered saline (PBS) 3 times and fixed with 4% paraformaldehyde for 15 minutes. For intracellular antigens, cells were permeabilized with 0.5% Triton X-100 for 20 minutes. Samples were blocked with goat serum (ZSGB-BIO, Beiing, China) in PBS with 2% bovine serum albumin for 30 minutes at room temperature followed by overnight incubation of the anti-DLL4 primary antibodies (MAB1506, R&D System Inc., MN) at 4°C. Secondary Alexa Fluor 594–conjugated goat anti-mouse antibody (SA00006-3; Proteintech Group, Inc., IL) in PBS was added to the slides, which were then incubated for 1 hour in darkness at 37°C. DAPI was used to stain the nuclear for 5 minutes, following which the cells were mounted onto an antifade reagent medium. The cells were imaged using fluorescence microscope (Olympus BX53, Tokyo, Japan).

Annexin V Detection of Apoptotic Cells

Apoptotic cells were identified using the Annexin V-PE/7-AAD detection kit. SGC7901-GFP cells (5× 10^5 cells/well) were seeded in 6-well plates. Following adherence to the dish, the cells were treated with 5 μg/ml anti-DLL4 antibody or 150 μg/ml DAPT, or a combination of anti-DLL4 antibody (5μg/ml) and DAPT (150 μg/ml) for 48 hours. Cells were digested by 0.25% trypsin without EDTA (Thermo Fisher Scientific, CA) and then were stained using an Annexin V-PE/7-AAD apoptosis kit (Nanjing KeyGen BioTech, Nanjing, China) according to the manufacturer's instructions. Stained cells were identified and analyzed using flow cytometry (Becton Dickinson, NJ). Each experiment was performed in triplicate.

Cell Cycle Analysis

Cell cycle phase distribution was determined by staining DNA with propidium iodide (PI). SGC7901-GFP cells were seeded in 6-well plates and treated with 5 μg/ml anti-DLL4 antibody

(BIOLEGEND) or 150 μg/ml DAPT (BIOLEGEND), or a combination of anti-DLL4 antibody (5 μg/ml) and DAPT (150 μg/ml) for 48 hours. Cells were harvested and fixed in 70% ethanol overnight at −20°C. After washing them 3 times with PBS, cells incubated with 50 μg/ml RNase (Nanjing KeyGen BioTech, Nanjing, China) and then stained with 50 μg/ml PI for 30 minutes at 4°C in the darkness. DNA contents were detected by flow cytometry and analyzed by CANTO-II (BD, NJ)

Cell Invasion Assay

For the invasion assay, the upper Transwell chamber of an insert was coated with 20 μl of 20% Matrigel (BD, NJ) in an RPMI1640 medium. After a drying time of 2 hours, the SGC7901-GFP cells (1×10^5 cells/well) were seeded in the upper chamber coated by Matrigel. Cells were treated with 5 μg/ml anti-DLL4 antibody or 150 μg/ml DAPT, or a combination of anti-DLL4 antibody (5 μg/ml) and DAPT (150 μg/ml). Afterward, 600 μl of medium containing 20% fetal bovine serum was added to the lower chamber. After 48 hours of incubation, the cells were washed twice with PBS and fixed with ethanol for 20 minutes. The leftover cells on the upper membrane were removed with cotton wool, and the cells that had invaded through the membrane were stained with crystal violet. After staining was done, cells on the back of the Transwell membrane were imaged and counted using an inverted microscope (Olympus BX53, Tokyo, Japan).

Animal Care

Thirty BALB/C female nude mice, aged 4 to 6 weeks and weighing 20 to 25 g, were obtained from the Yang Zhou University Laboratory Animal Center (SCXK. Su. 20120004). All mice were maintained in a HEPA-filtered environment at 24°C to 25°C, and humidity was maintained at 50% to 60%. All animals were fed an autoclaved laboratory rodent diet. Animal experiments were approved by the Animal Committee of Nanjing Origin Biosciences, China (OB1607).

Orthotopic Mouse Model of Gastric Cancer

SGC7901-GFP human gastric cancer cells were harvested at 80% confluence by 0.25% trypsin digestion. The stock tumor was established by subcutaneously injecting SGC7901-GFP cells (5×10^6) into the flank of the nude in mice. Tumors grown in the mice were harvested at the exponential growth phase and resected under aseptic conditions. Strong GFP expression in the SGC7901-GFP tumor tissue was confirmed by fluorescence microscopy. Necrotic tissues were removed, and viable tissue was cut with scissors and minced into 1-mm^3 pieces. The surgical orthotopic implantation method used in this study was similar to previous published procedures [23]. Animals were anesthetized by injection of a 0.02-ml solution of 50% ketamine, 38% xylazine, and 12% acepromazine maleate. All surgical procedures and animal manipulations were conducted under aseptic conditions in a HEPA-filtered laminar-flow hood under a surgical microscope (Model YZ20P5, Shanghai Precision Instruments, Shanghai, China).

UTMD Treatment

To increase the efficiency of drug delivery *in vivo*, UTMD technique was used to deliver the anti-DLL4 antibody and DAPT therapy. Forty-eight tumor-bearing mice were randomly divided into 5 groups of 6 mice each once the average tumor size had reached 100 mm^3. Group 1 served as untreated control. Group 2 served as UTMD control and received unconjugated microbubbles (MB) and UTMD (MB +UTMD). Group 3 received anti-DLL4 antibody conjugated microbubbles (MBd) and UTMD (MBd+UTMD). Group 4 received MB, DAPT, and UTMD (MB+DAPT+UTMD). Group 5 received MBd, DAPT, and UTMD (MBd+DAPT+UTMD). Mice were anesthetized with ketamine, acepromazine, and xylazine and then placed in a supine position on a heated stage. Ultrasound imaging was performed using a Siemens Sequoia 512 ultrasound scanner with a 15L-8 linear transducer (Siemens, Mountain View, CA) to localize the orthotropic gastric tumor for subsequent UTMD. The transducer was coupled to the mouse skin in the upper abdominal region with an acoustic coupling agent. A conventional B-mode ultrasound scan without contrast agents was first conducted to determine the location, size, and baseline echogenicity of the tumor. Color Doppler flow imaging was then performed to visualize the blood flow in the gastric tumor. The scanner was then placed in the contrast imaging mode (Cadence CPS), and the gain and MI settings were optimized to enable noninvasive detection of microbubble agents. MB and MBd were administered as a 50-μl (approximately 1.2×10^7 microbubbles per dose) bolus by retro-orbital injection. For DAPT administration, 400 μg of DAPT was combined with 50 μl of either MB or MBd, which was administered to the MB+DAPT+UTMD and MBd+DAPT+UTMD groups, respectively. Nondestructive contrast ultrasound imaging was performed both before and after UTMD treatment in order to verify the delivery and complete clearance of microbubbles within the tumor. UTMD was performed using a hand-held sonoporator (Sonitron 2000, Artison, OK). This device consists of a piezoelectric transducer with a center frequency of 1 MHz. The transducer was placed above the ventral midline of the abdominal and thoracic cavities with the ultrasound coupling gel. The settings were optimized as follows: 50% duty cycle, treatment duration of 30 seconds, and an acoustic intensity of 2 W/cm^2. The sonoporator was set to 30-second on/off cycles to enable complete reperfusion of the microbubbles into the aortas following each 30-second cycle of UTMD. This process was repeated three times. All treatments and UTMD were administered on a daily basis, 3 times a day, using the same doses and settings.

Real-Time In Vivo Fluorescence Imaging

Tumor growth was measured through real-time *in vivo* fluorescence imaging using a fluorescence stereo microscope (MZ650; Nanjing Optic Instrument Inc., Nanjing, China) equipped with bandpass HQ600/50 emission and HQ540/40 excitation filters (Chroma Technology, Brattleboro, VT). Animal body weights and clinical signs were recorded over the course of the experiments. All animals were sacrificed 18 days after initiation of treatments. At autopsy, the tumor was removed and weighed. Images were processed and analyzed using IMAGE PRO Plus 6.0 software (Media Cybernetics, Silver Spring, MD).

TUNEL Detection of Apoptosis

Apoptosis of the tumor cells following treatments *in vivo* was determined by TUNEL staining using a commercially available kit (In Situ Cell Death Detection Kit, POD; Roche, Germany). Tumor sections were deparaffinized and dehydrated according to standard protocols. Tissue sections were incubated with Proteinase K working solution for 30 minutes at 21°C to 37°C. The slides were then washed twice with PBS (pH 7.2-7.6). The positive control was incubated with DNase I for 10 minutes at 15°C to 25°C, and the negative control was incubated with label solution (without terminal transferase) instead of the TUNEL reaction mixture. The slides were then washed three times with PBS (pH 7.2-7.6). Converter-POD was added to the slides which were then incubated in a

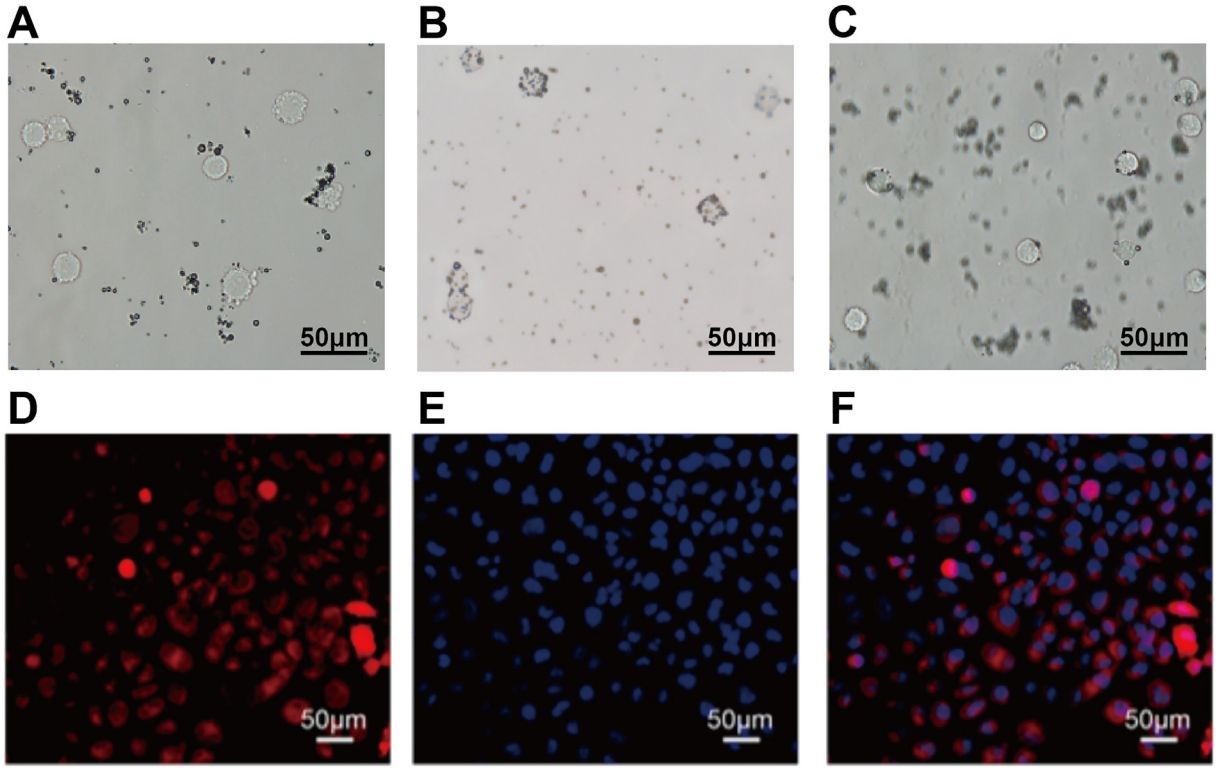

Figure 1. DLL4 protein expression in SGC-7901-GFP cells. Membranous expression pattern of DLL4 protein in SGC-7901 cells detected by the rosette formation test with anti-DLL4 antibody conjugated microbubbles. (A) No rosette formation observed with SGC-7901 cells treated with unconjugated microbubbles. (B) Rosette-like structure formed with SGC-7901 cells treated with anti-DLL4 antibody conjugated microbubbles. (C) Rosette formation blocked by adding anti-DLL4 antibody prior to SGC-7901 cells being treated with anti-DLL4 antibody conjugated microbubbles. Bars = 50 μm. DLL4 expression in SGC-7901 cells was detected by immunofluorescence. (D) Red fluorescence showing DLL4 expression in SGC-7901 cells. (E) DAPI showing SGC-7901 nuclei. (F) Merged image of A and B.

humidified chamber for 30 minutes at 37°C. Following this, the slides were washed three times with PBS (pH 7.2-7.6). The 3,3-diaminobenzidine substrate was added onto the slides and incubated for 10 minutes at 15°C to 25°C, after which they were then washed three times with PBS (pH 7.2-7.6). The slides were then mounted and analyzed through the microscope (Olympus, Melville, NY, USA). The slides were viewed at 400× magnification, and apoptotic cells were identified by the brown-stained appearance of the cells. Expression levels were quantified based on the average optical density (AOD) of the positive cells in five fields/sample using the Image-Pro Plus 6.0 software.

Immunohistochemistry

Tumor tissue was fixed in 10% formalin, dehydrated, paraffin-embedded, and sectioned into 4-μm blocks. For each animal, a single microscope slide with three sections of the paraffin block was made. The sections were washed three times with PBS for 5 minutes each, blot dried, and then treated with 3% hydrogen peroxide for 30 minutes at room temperature to block endogenous peroxidase activity. The sections were immersed in an antigen-retrieval solution (citrate buffer, pH 6.0) for 10 minutes followed by rinse with PBS. After blocking with normal goat serum for 30 minutes at 37°C, sections were incubated overnight with primary antibodies against BAX, BCL-2, and P53 (BD Biosciences, San Diego, CA) (1:100 dilution in PBS). Following this, the sections were also incubated with a peroxidase-conjugated anti-rabbit IgG secondary antibody (Biosynthesis Biotechnology Co., Ltd.) for 1 hour at room temperature. Subsequently, the sections were incubated with 3,3-diaminobenzidine reagent (ZSGB-BIO, Beijing, P.R. China) for 10 minutes, counterstained with hematoxylin, dehydrated, and mounted for microscopy. The slides were viewed at 100× or 400× magnification with positive cells identified by the brown-stained appearance of the cells. Expression levels were quantified based on the AOD of the positive cells in five fields/sample using the Image-Pro Plus 6.0 software.

Statistical Analysis

Data are expressed as mean ± SD, and a one-way analysis of variance was done using SPSS software version 19.0. A P value < .05 was considered to be statistically significant.

Results

DLL4 Protein Expression in Gastric Cancer Cells

We detected DLL4 expression in the SGC-7901-GFP gastric cancer cells using the rosette formation test and immunofluorescence staining. Our results showed that the SGC-7901-GFP cells did not attach to the unconjugated microbubbles (Figure 1*A*). By contrast, the cytomembranes of the SGC-7901 cells were extensively bound to the DLL4 antibody conjugated microbubbles and formed a rosette-like circle (Figure 1*B*). This phenomenon could be abolished while the SGC-7901-GFP cells were blocked with DLL4 antibody prior to the addition of DLL4 targeted microbubbles (Figure 1*C*). The immunofluorescence detection further confirmed the expression of DLL4 in the SGC-7901-GFP cells (Figure 1, *D-F*). These results verified that the DLL4 protein is expressed and located in the membrane of SGC-7901-GFP gastric cancer cells.

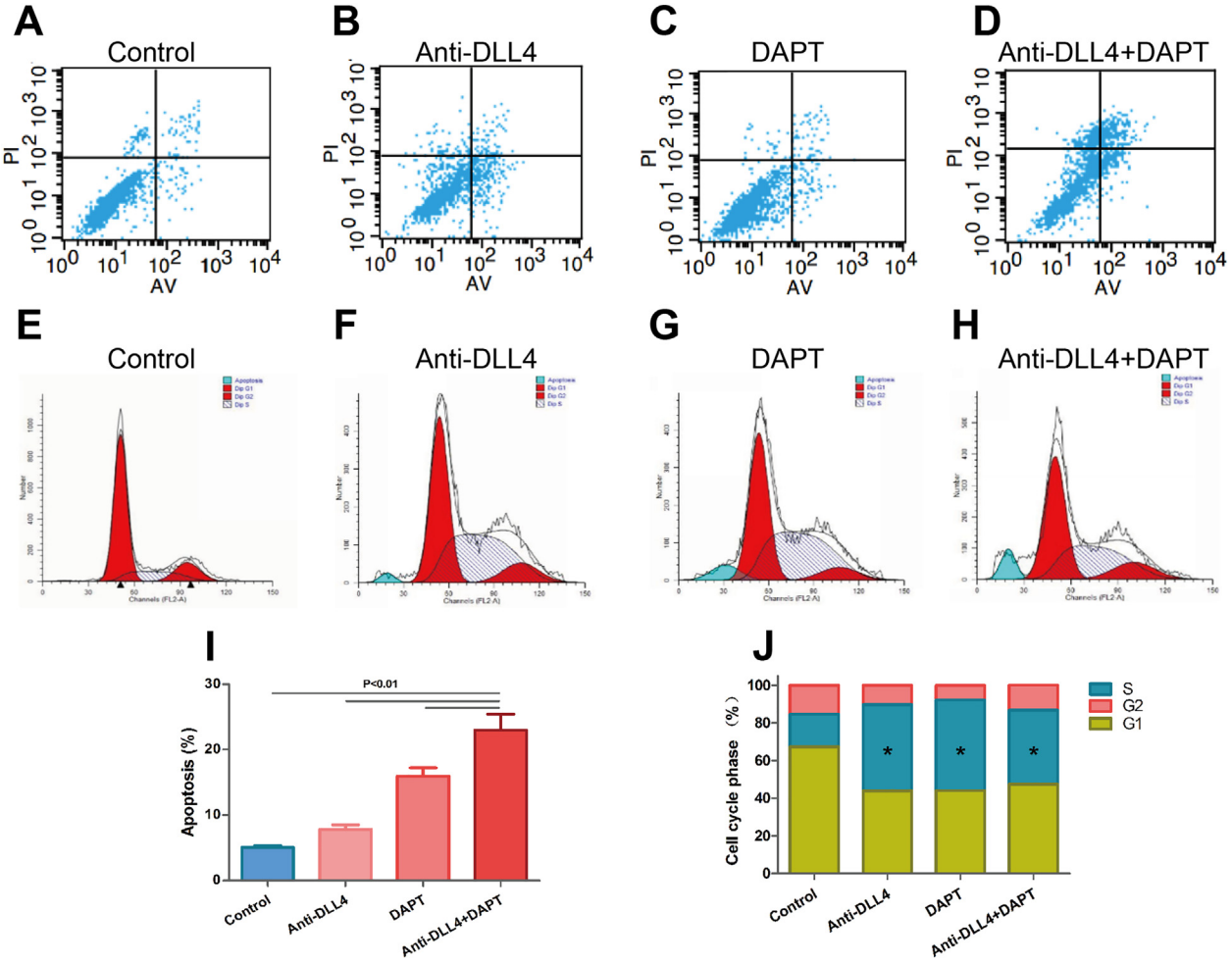

Figure 2. Effect of anti-DLL4 and DAPT on apoptosis and cell cycle in gastric cancer cells. (A to D) Cells were stained with Annexin V and PI, following which cell apoptosis in each group was detected by flow cytometry. (E to H) Cell cycle phase distribution was measured by staining DNA with PI followed by flow cytometry. (I and J) Cell apoptosis rate and cell cycle distribution in each group were analyzed. *$P <$ .01, when compared with control group.

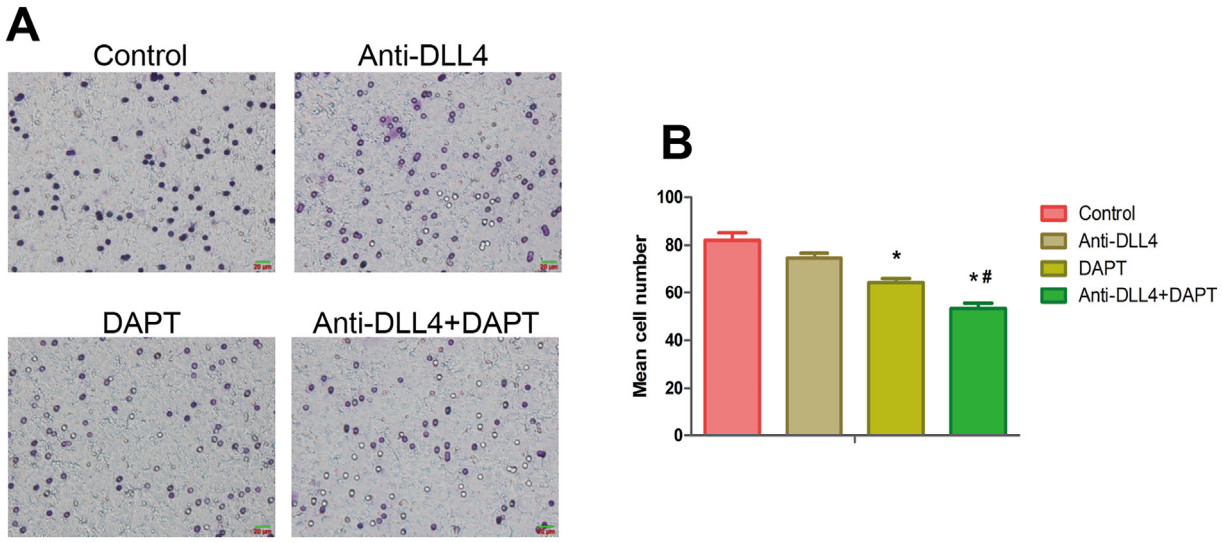

Figure 3. Effect of anti-DLL4 and DAPT on cell invasion of gastric cancer cells. Cell invasion was assessed by Transwell invasion assay. (A) Representative Transwell cells images in each group. (B) Comparison of immigrated cell numbers in each group. *$P <$ .01, when compared to control group. #$P <$ .01, when compared to DAPT group.

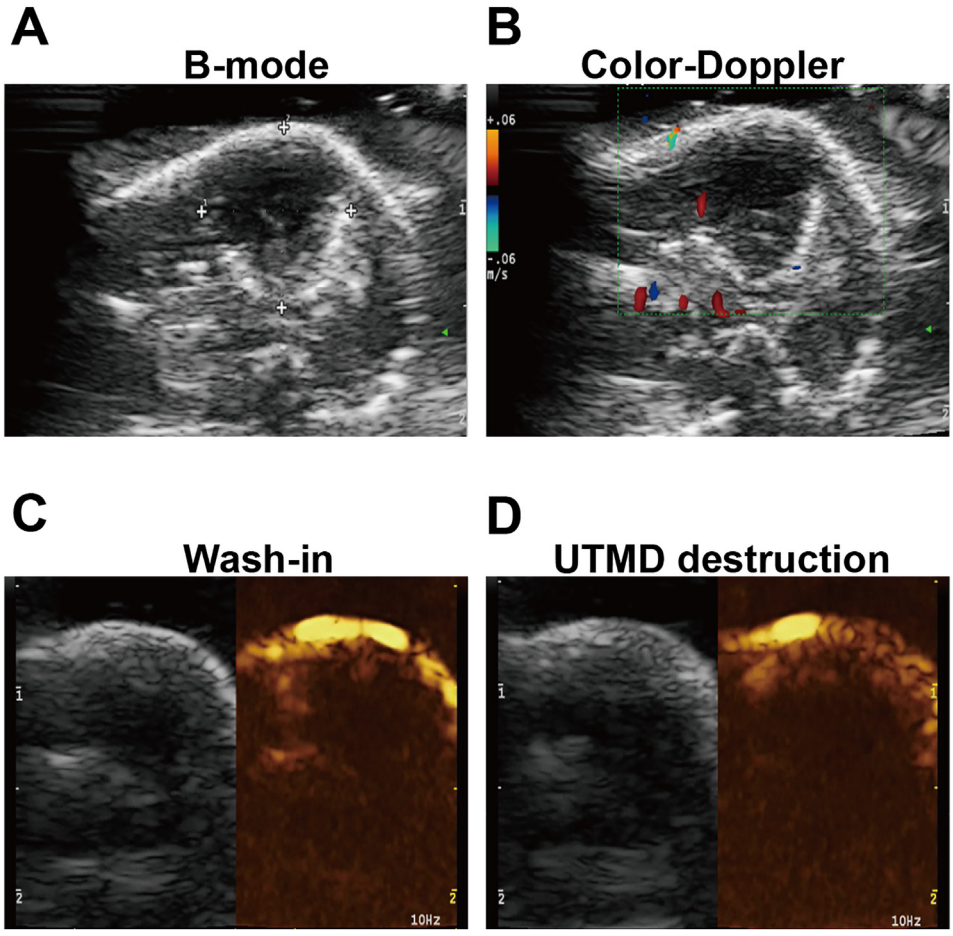

Figure 4. Conventional ultrasound imaging and contrast-enhanced ultrasound imaging of orthotopic gastric tumor in mice for UTMD. (A) B-mode imaging of tumor. (B) Color Doppler imaging of blood flow in tumor. (C) CPS mode imaging of microbubble wash-in in tumor. (D) CPS mode imaging of microbubble destruction in tumor by UTMD.

DAPT Enhanced Anti-DLL4–Induced Apoptosis in Gastric Cancer Cells

SGC-7901-GFP gastric cancer cells were treated with the anti-DLL4 antibody, DAPT, or a combination of anti-DLL4 antibody and DAPT. Cell apoptosis was assessed using flow cytometry. As shown in Figure 2, *A-D*, SGC-7901-GFP cells in the anti-DLL4–, DAPT-, and anti-DLL4+DAPT–treated groups showed an increased early apoptosis rate as compared to untreated group. The anti-DLL4+DAPT–treated group showed a significantly higher apoptosis rate than that of either the anti-DLL4– or DAPT-treated group (Figure 2*I*, $P < .01$), indicating the synergetic effect of anti-DLL4+DAPT treatment on the induction of tumor cell apoptosis.

Conversely, anti-DLL4–, DAPT-, and anti-DLL4+DAPT–treated groups showed decreased cell distribution in the G1 phase and increased cell distribution in the S phase when compared to the untreated group (Figure 2, *E-H*). Simultaneously, cell distribution in the phase G2 was significantly lower in the treatment groups (Figure 2*J*, $P < .01$). However, no synergy was observed in the cell cycle arrest assays.

Suppressed Invasive Capabilities in Gastric Cancer Cells

Effect of anti-DLL4 and DAPT therapy on cell invasion was assessed using the Transwell invasion assay. As shown in Figure 3, therapy with DAPT alone or a combination of anti-DLL4 and DAPT resulted in a significant decrease in the invasion of SGC-7901-GFP cells ($P < .01$). However, no significant differences were found between the anti-DLL4–treated group and control group ($P > .05$). The anti-DLL4+DAPT–treated group showed significantly greater inhibition in cell invasion than DAPT-treated group ($P < .01$), suggesting the synergetic effect of the combined treatment of anti-DLL4 and DAPT on cell invasion.

Synergistic Antitumor Effect in Orthotopic Gastric Tumor Models

UTMD was used for *in vivo* administration of anti-DLL4 antibody and DAPT. As shown in Figure 4, neoplastic formation and functional blood perfusion were confirmed by B mode (Figure 4*A*) and color Doppler (Figure 4*B*) imaging for all orthotopic animal models. After the injection of microbubbles, accumulation in the targeted area of the tumor was significantly enhanced (Figure 4*C*). After each 30-second cycle of UTMD, the microbubbles were destroyed (Figure 4*D*).

The effect of anti-DLL4 antibody and DAPT on tumor growth in orthotopic models of gastric cancer was evaluated using real-time *in vivo* fluorescence imaging. Tumor size was measured on days 0, 4, 8, 11, 15, and 18 following treatments. Representative fluorescence images are shown in Figure 5*A*. Furthermore, H&E staining demonstrated that therapy with both unconjugated microbubbles (MB)+DAPT+UTMD and anti-DLL4 antibody conjugated

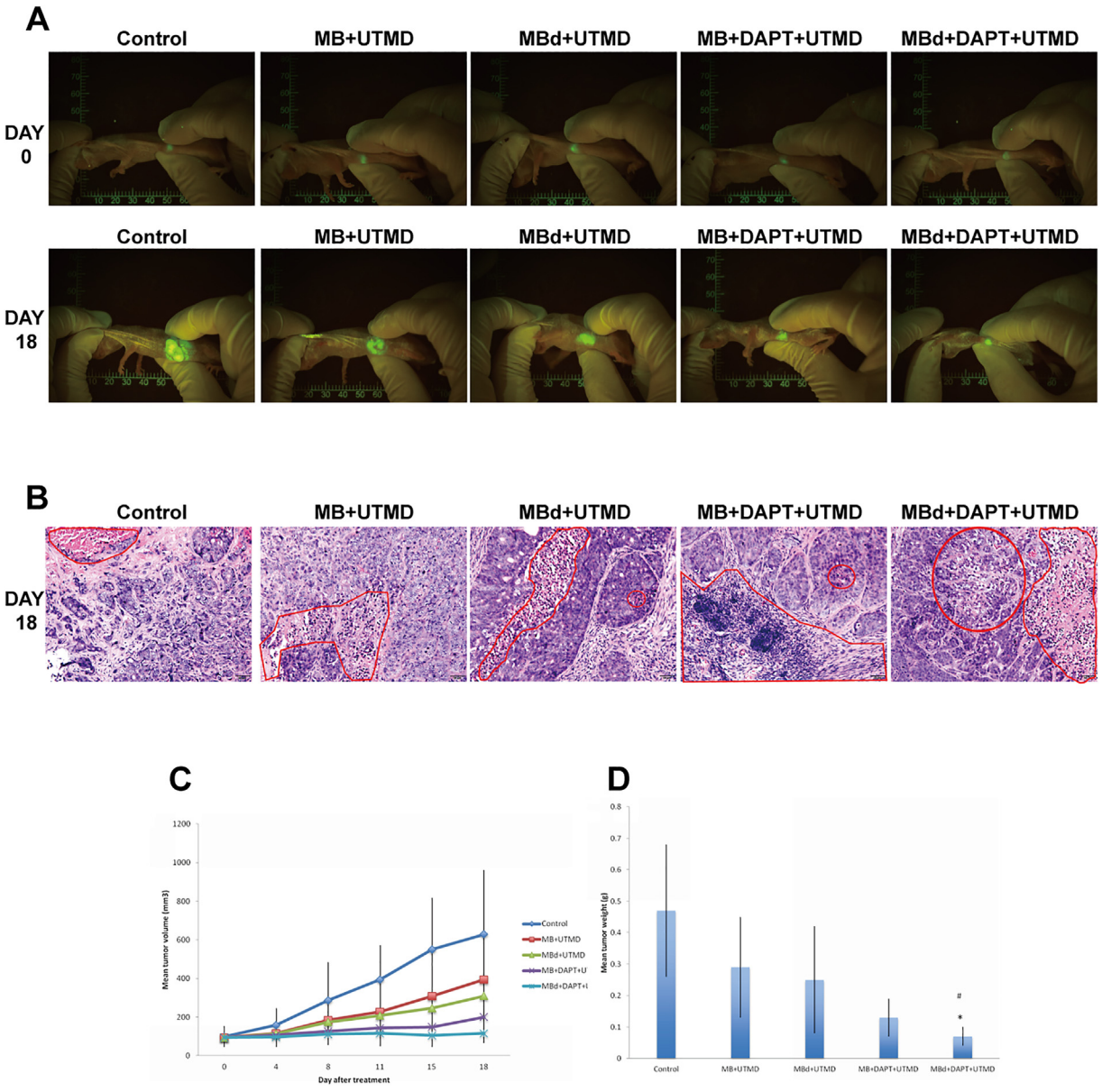

Figure 5. Effect of anti-DLL4 and DAPT on tumor growth in orthotopic gastric tumor models. Tumor growth was monitored and quantified by real-time whole-body fluorescence imaging. Final tumor weight was determined at autopsy. (A) *In vivo* whole-body fluorescence imaging of tumor before treatment and 18 days after treatment in each group. (B) Markedly increased necrogenous reaction in the parenchymal of tumor in the combined treatment group was observed by H&E staining. (C) Tumor growth curves in each group. (D) Final tumor weights at the end of the study period in each group. *$P < .01$, when compared to MB+UTMD control. #$P < .01$, when compared to MB+DAPT+UTMD group.

microbubbles (MBd)+DAPT+UTMD can effectively induce necrogenous reaction in the parenchyma of orthotopic tumor (Figure 5*B*). This was reflected by simultaneous reduction in tumor size and tumor weight in the above groups ($P < .01$, Figure 5, *C* and *D*), especially in the MBd+DAPT+UTMD group. However, no significant tumor growth inhibition was found in the MBd+UTMD group when compared to the MB+UTMD control group ($P > .05$). These results strongly point towards the synergistic *in vivo* antitumor effect of the anti-DLL4 and DAPT combined therapy.

In Vivo Tumor Cell Apoptosis Caused by Synergic Treatment

The effect of anti-DLL4 and DAPT on tumor cell apoptosis was analyzed by TUNEL staining. TUNEL-positive cells were analyzed only in regions of intact tumor, while carefully avoiding the central necrosis typically observed in xenografts. Representative fields of view and quantification from each group are shown in Figure 6. Tumor cell apoptosis was significantly increased by MB+DAPT+UTMD and MBd+DAPT+UTMD treatments in comparison to the MB+UTMD control ($P < .05$). However, the MBd+UTMD group did not show significantly increased tumor cell apoptosis when compared to the MB+UTMD control group ($P > .05$). On the other hand, significant tumor cell apoptosis was observed in MBd+DAPT+UTMD group ($P < .05$), suggesting that the combination treatment has a synergetic *in vivo* proapoptotic effect.

Aberrant Expression of Apoptosis-Related Genes in In Vivo Tumor Cells

Immunohistochemical staining was performed to assess the effect of anti-DLL4 and DAPT on the expression of apoptosis-related genes BAX, Bcl-2, and P53. Representative fields of view for each gene from

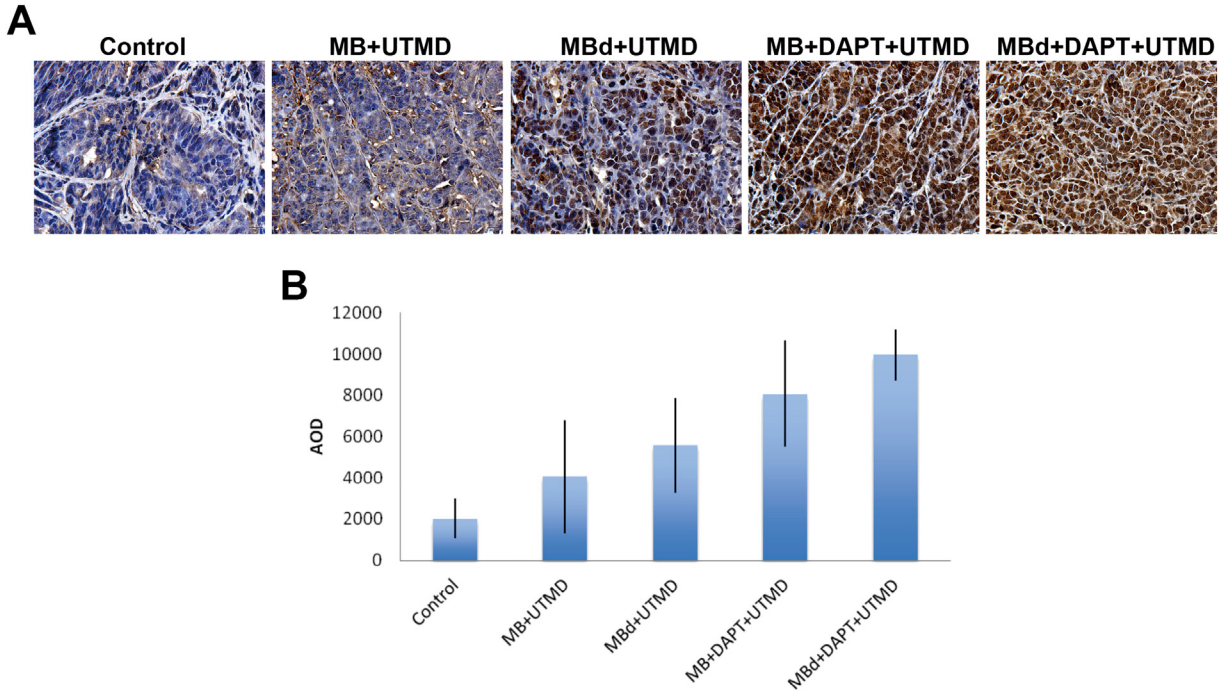

Figure 6. Effect of anti-DLL4 and DAPT on tumor cell apoptosis in *in vivo* models. The apoptosis of the tumor cells was detected by TUNEL staining. (A) Representative TUNEL images for cell apoptosis in each group (100× magnification). (B) Quantitation of cell apoptosis by AOD. *$P < .01$, when compared to the MB+UTMD control. #$P < .01$, when compared to the MB+DAPT+UTMD group.

each group are shown in Figure 7*A*. The MBd+UTMD group only showed a significant increase in the expression of BAX gene ($P < .05$), but no effects on the expression of Bcl-2 and P53 genes were observed when compared to the MB+UTMD control group. MB+DAPT+UTMD treatment significantly increased the expression of the BAX and P53 genes ($P < .05$) but did not have effect on the expression of Bcl-2 when compared to the MB+UTMD control group. However, MBd+DAPT+UTMD group showed significantly increased expression of the BAX and P53 genes and reduced Bcl-2 ($P < .05$), suggesting that the reduction of Bcl-2 expression may be attributed to the synergetic antitumor and proapoptotic effects of the combination therapy (Figure 7*B*).

Body Weight Measurement of the Animals

Clinical observation and body weight measurement of the animals were done to assess the toxicity of anti-DLL4 and DAPT treatments. As shown in Figure 7*C*, all groups showed approximately 10% loss of body weight by the end of the study period. No significant differences in the final body weight were found between the treated groups and untreated control groups ($P > .05$), indicating the body weight loss is more likely attributed to the tumor burden rather than treatment.

Discussion

DLL4 expression is closely related to the TNM stage, node stage, and distant metastasis of the tumor and indicates poor prognosis in cancer patients [12]. GSIs have been recognized for their antitumor effects in many cancers. These effects include inhibition of the cell proliferation, increased apoptosis, and decreased cell invasion [20]. In this study, we aimed to investigate whether anti-DLL4 treatment can enhance the antitumor effects of GSI in gastric cancer. We chose SGC7901 gastric cancer cells as the study object because of its high expression of DLL4, which was confirmed by rosette formation test and immunofluorescence. The results of the *in vitro* study demonstrated that the combination treatment of anti-DLL4 and DAPT leads to a higher rate of cell apoptosis and greater cell invasion inhibition when compared to DAPT treatment alone. It has been reported that DLL4-induced Notch activation is linked to tumor-initiating cell proliferation [17,24]. Yano et al. [25] reported that cancer cells in G0/G1 phase in Gelfoam histoculture migrated further and more rapidly than cancer cells in the S/G2/M phase. Following entry into the S/G2/M phases, cancer cells ceased migration and only began migrating again when the cells reentered G0/G1. Therefore, one of the mechanisms by which anti-DLL4 and DAPT treatment inhibits cell invasion may be through its increased S-phase cell arresting effect.

In order to confirm our *in vitro* observations and to evaluate the antitumor efficacy of anti-DLL4 and DAPT *in vivo*, we analyzed their effects on tumor growth and tumor cell apoptosis in an orthotopic mouse model of gastric cancer. UTMD was used to enhance the delivery of anti-DLL4 antibody and DAPT. Therapeutic UTMD has shown great potential as a tool for targeted disruption of tumor vasculature [26,27]. UTMD is a process in which acoustic energy induces bubble collapse, generating microjets that create transient pores in the cell membrane and facilitate transport of large molecules into the cell cytoplasm [28,29]. This technique is being explored for gene transfection and targeted drug delivery and release [30,31]. Our study revealed that the combined therapy of anti-DLL4 and DAPT has synergetic antitumor efficacy and proapoptotic effects, greater than those produced by DAPT treatment alone.

To further investigate the molecular mechanisms underlying these antitumor and proapoptotic effects, we measured the expression of

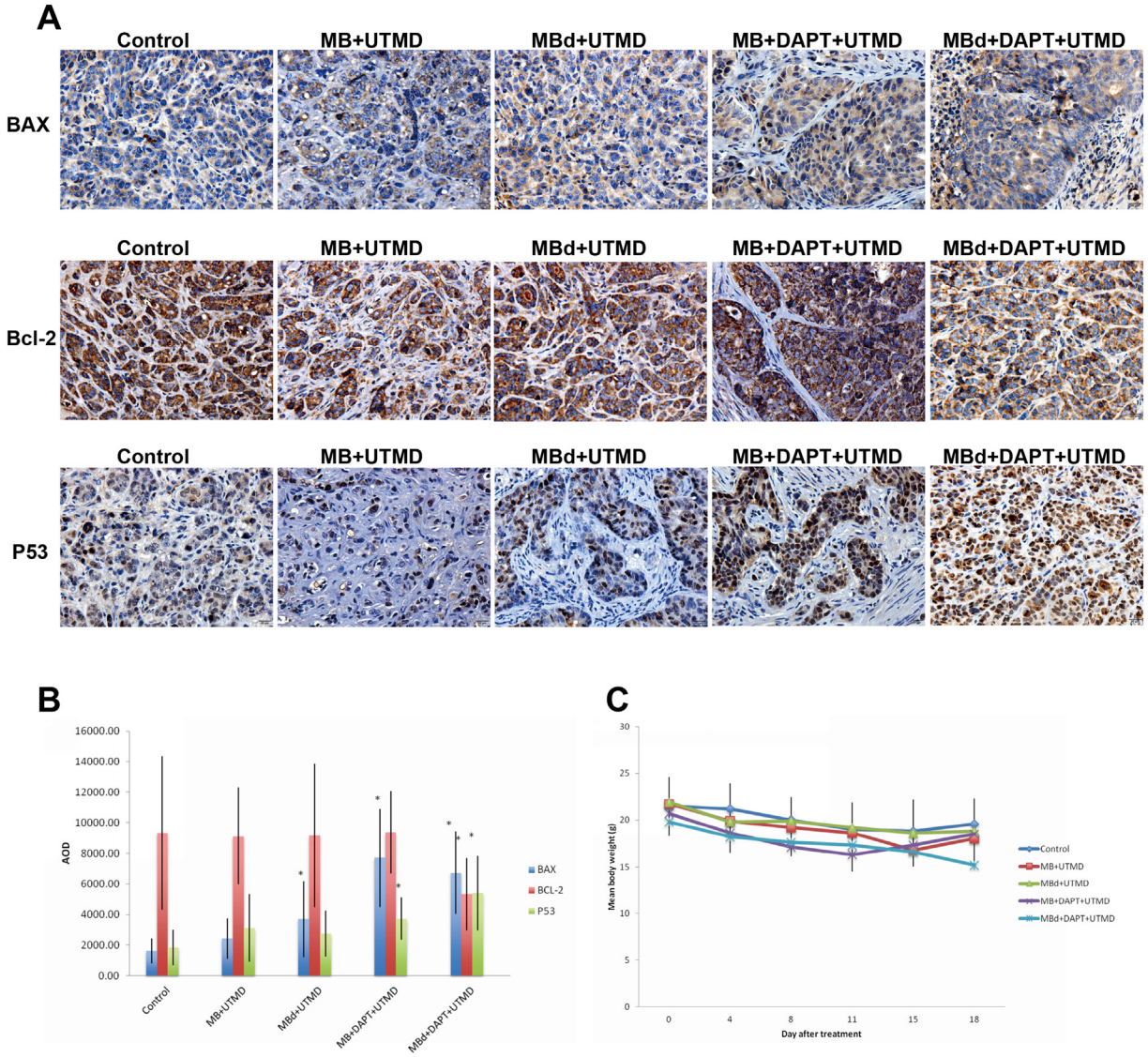

Figure 7. Effect of anti-DLL4 and DAPT on the expression of apoptosis-related genes and the body weight of mice in orthotopic gastric tumor models. (A) Representative immunohistochemistry staining for BAX, Bcl-2, and P53 in the tumors of each group. 400× magnification. (B) AOD of immunohistochemistry staining of tumor samples in each group. *$P < .05$, when compared to the MB+UTMD control. (C) No significant anti-DLL4– and DAPT-related body weight loss was observed in the treated mice.

the apoptosis-related proteins Bcl-2 and BAX and the tumor suppressor protein P53. It is known that cancer development and progression are attributed to destruction of the balance between cell proliferation and apoptosis [32]. Apoptosis is mediated by several cascade proteins, especially members of the Bcl-2 family and BAX [33]. It is believed that the Bcl-2 gene product inhibits cell death and contributes to the prolongation of cell survival, while BAX (Bcl-2 antagonist X), an important homologue of Bcl-2, is a promoter of apoptosis [34,35]. Evidently, the BAX/Bcl-2 ratio plays a vital role in the fate of the cell. The transcriptional function of P53 is considered a marker of the expression of various genes involved in cell cycle arrest, leading to cell apoptosis [36]. Research suggests that some anticancer agents induce apoptotic cell death in NSCLC cells through upregulation of p53 and p21 [37]. In the present study, we observed that DAPT treatment alone increased the expression BAX and P53, while the combined treatment of anti-DLL4 and DAPT reduced Bcl-2 expression in addition to increasing expression of BAX and P53. These alterations in the expression of BAX and Bcl-2 give rise to a high BAX/Bcl-2 ratio, which is considered to significantly increase the cell's susceptibility to apoptosis. Higher BAX/Bcl-2 ratios resulted in a higher proportion of apoptotic cells in the combined treatment group when compared to that in the DAPT-treated group. At least a part of the apoptosis-promoting effect of anti-DLL4 and DAPT on SGC7901gastric cancer cells may be attributed to the regulation of Bcl-2 and BAX, as well as p53 activation.

Conclusions

Concurrent treatment with anti-DLL4 enhances the antitumor and proapoptotic efficacy of the γ-secretase inhibitor in gastric cancer both *in vitro* and *in vivo*. Regulation of the apoptosis-related proteins Bcl-2 and BAX and tumor suppressor protein P53 may be one of the underlying mechanisms of these antitumor and proapoptotic effects.

References

[1] Siegel RL, Miller KD, and Jemal A (2016). Cancer statistics, 2016. *CA Cancer J Clin* **66**, 7–30.

[2] Allemani C, Weir HK, Carreira H, Harewood R, Spika D, Wang XS, Bannon F, Ahn JV, Johnson CJ, and Bonaventure A, et al (2015). Global surveillance of cancer survival 1995-2009: analysis of individual data for 25,676,887 patients from 279 population-based registries in 67 countries (CONCORD-2). *Lancet* **385**, 977–1010.

[3] Thiel A and Ristimaki A (2012). Gastric cancer: basic aspects. *Helicobacter* **17** (Suppl. 1), 26–29.

[4] Guruharsha KG, Kankel MW, and Artavanis-Tsakonas S (2012). The Notch signalling system: recent insights into the complexity of a conserved pathway. *Nat Rev Genet* **13**, 654–666.

[5] Kim TH and Shivdasani RA (2011). Notch signaling in stomach epithelial stem cell homeostasis. *J Exp Med* **208**, 677–688.

[6] Brzozowa M, Mielanczyk L, Michalski M, Malinowski L, Kowalczyk-Ziomek G, Helewski K, Harabin-Slowinska M, and Wojnicz R (2013). Role of Notch signaling pathway in gastric cancer pathogenesis. *Contemp Oncol (Pozn)* **17**, 1–5.

[7] Kang M, Jiang B, Xu B, Lu W, Guo Q, Xie Q, Zhang B, Dong X, Chen D, and Wu Y (2013). Delta like ligand 4 induces impaired chemo-drug delivery and enhanced chemoresistance in pancreatic cancer. *Cancer Lett* **330**, 11–21.

[8] Mori M, Miyamoto T, Yakushiji H, Ohno S, Miyake Y, Sakaguchi T, Hattori M, Hongo A, Nakaizumi A, and Ueda M, et al (2012). Effects of N-[N-(3, 5-difluorophenacetyl-L-alanyl)]-S-phenylglycine t-butyl ester (DAPT) on cell proliferation and apoptosis in Ishikawa endometrial cancer cells. *Hum Cell* **25**, 9–15.

[9] Subramaniam D, Ponnurangam S, Ramamoorthy P, Standing D, Battafarano RJ, Anant S, and Sharma P (2012). Curcumin induces cell death in esophageal cancer cells through modulating Notch signaling. *PLoS One* **7**, e30590.

[10] Yoneya T, Tahara T, Nagao K, Yamada Y, Yamamoto T, Osawa M, Miyatani S, and Nishikawa M (2001). Molecular cloning of delta-4, a new mouse and human Notch ligand. *J Biochem* **129**, 27–34.

[11] Shutter JR, Scully S, Fan W, Richards WG, Kitajewski J, Deblandre GA, Kintner CR, and Stark KL (2000). Dll4, a novel Notch ligand expressed in arterial endothelium. *Genes Dev* **14**, 1313–1318.

[12] Zhang JX, Cai MB, Wang XP, Duan LP, Shao Q, Tong ZT, Liao DZ, Li YY, Huang MY, and Zeng YX, et al (2013). Elevated DLL4 expression is correlated with VEGF and predicts poor prognosis of nasopharyngeal carcinoma. *Med Oncol* **30**, 390.

[13] Chen HT, Cai QC, Zheng JM, Man XH, Jiang H, Song B, Jin G, Zhu W, and Li ZS (2012). High expression of delta-like ligand 4 predicts poor prognosis after curative resection for pancreatic cancer. *Ann Surg Oncol* **19**(Suppl. 3), S464–474.

[14] Leslie JD, Ariza-McNaughton L, Bermange AL, McAdow R, Johnson SL, and Lewis J (2007). Endothelial signalling by the Notch ligand Delta-like 4 restricts angiogenesis. *Development* **134**, 839–844.

[15] Kuhnert F, Kirshner JR, and Thurston G (2011). Dll4-Notch signaling as a therapeutic target in tumor angiogenesis. *Vasc Cell* **3**, 20.

[16] Sainson RC and Harris AL (2007). Anti-Dll4 therapy: can we block tumour growth by increasing angiogenesis? *Trends Mol Med* **13**, 389–395.

[17] Hoey T, Yen WC, Axelrod F, Basi J, Donigian L, Dylla S, Fitch-Bruhns M, Lazetic S, Park IK, and Sato A, et al (2009). DLL4 blockade inhibits tumor growth and reduces tumor-initiating cell frequency. *Cell Stem Cell* **5**, 168–177.

[18] Kuramoto T, Goto H, Mitsuhashi A, Tabata S, Ogawa H, Uehara H, Saijo A, Kakiuchi S, Maekawa Y, and Yasutomo K, et al (2012). Dll4-Fc, an inhibitor of Dll4-notch signaling, suppresses liver metastasis of small cell lung cancer cells through the downregulation of the NF-kappaB activity. *Mol Cancer Ther* **11**, 2578–2587.

[19] Jenkins DW, Ross S, Veldman-Jones M, Foltz IN, Clavette BC, Manchulenko K, Eberlein C, Kendrew J, Petteruti P, and Cho S, et al (2012). MEDI0639: a novel therapeutic antibody targeting Dll4 modulates endothelial cell function and angiogenesis in vivo. *Mol Cancer Ther* **11**, 1650–1660.

[20] Katoh M and Katoh M (2007). Notch signaling in gastrointestinal tract (review). *Int J Oncol* **30**, 247–251.

[21] Li LC, Peng Y, Liu YM, Wang LL, and Wu XL (2014). Gastric cancer cell growth and epithelial-mesenchymal transition are inhibited by gamma-secretase inhibitor DAPT. *Oncol Lett* **7**, 2160–2164.

[22] Li GG, Li L, Li C, Ye LY, Li XW, Liu DR, Bao Q, Zheng YX, Xiang DP, and Chen L, et al (2013). Influence of up-regulation of Notch ligand DLL4 on biological behaviors of human gastric cancer cells. *World J Gastroenterol* **19**, 4486–4494.

[23] Furukawa T, Fu X, Kubota T, Watanabe M, Kitajima M, and Hoffman RM (1993). Nude mouse metastatic models of human stomach cancer constructed using orthotopic implantation of histologically intact tissue. *Cancer Res* **53**, 1204–1208.

[24] Fischer M, Yen WC, Kapoun AM, Wang M, O'Young G, Lewicki J, Gurney A, and Hoey T (2011). Anti-DLL4 inhibits growth and reduces tumor-initiating cell frequency in colorectal tumors with oncogenic KRAS mutations. *Cancer Res* **71**, 1520–1525.

[25] Yano S, Zhang Y, Miwa S, Tome Y, Hiroshima Y, Uehara F, Yamamoto M, Suetsugu A, Kishimoto H, and Tazawa H, et al (2014). Spatial-temporal FUCCI imaging of each cell in a tumor demonstrates locational dependence of cell cycle dynamics and chemoresponsiveness. *Cell Cycle* **13**, 2110–2119.

[26] Smith AH, Fujii H, Kuliszewski MA, and Leong-Poi H (2011). Contrast ultrasound and targeted microbubbles: diagnostic and therapeutic applications for angiogenesis. *J Cardiovasc Transl Res* **4**, 404–415.

[27] Zhang C, Huang P, Zhang Y, Chen J, Shentu W, Sun Y, Yang Z, and Chen S (2014). Anti-tumor efficacy of ultrasonic cavitation is potentiated by concurrent delivery of anti-angiogenic drug in colon cancer. *Cancer Lett* **347**, 105–113.

[28] Tlaxca JL, Anderson CR, Klibanov AL, Lowrey B, Hossack JA, Alexander JS, Lawrence MB, and Rychak JJ (2010). Analysis of in vitro transfection by sonoporation using cationic and neutral microbubbles. *Ultrasound Med Biol* **36**, 1907–1918.

[29] Kinoshita M and Hynynen K (2005). Intracellular delivery of Bak BH3 peptide by microbubble-enhanced ultrasound. *Pharm Res* **22**, 716–720.

[30] Dittmar KM, Xie J, Hunter F, Trimble C, Bur M, Frenkel V, and Li KC (2005). Pulsed high-intensity focused ultrasound enhances systemic administration of naked DNA in squamous cell carcinoma model: initial experience. *Radiology* **235**, 541–546.

[31] Bekeredjian R, Chen S, Grayburn PA, and Shohet RV (2005). Augmentation of cardiac protein delivery using ultrasound targeted microbubble destruction. *Ultrasound Med Biol* **31**, 687–691.

[32] Evan GI and Vousden KH (2001). Proliferation, cell cycle and apoptosis in cancer. *Nature* **411**, 342–348.

[33] Youle RJ and Strasser A (2008). The BCL-2 protein family: opposing activities that mediate cell death. *Nat Rev Mol Cell Biol* **9**, 47–59.

[34] Golestani Eimani B, Sanati MH, Houshmand M, Ataei M, Akbarian F, and Shakhssalim N (2014). Expression and prognostic significance of bcl-2 and bax in the progression and clinical outcome of transitional bladder cell carcinoma. *Cell J* **15**, 356–363.

[35] Oltvai ZN, Milliman CL, and Korsmeyer SJ (1993). Bcl-2 heterodimerizes in vivo with a conserved homolog, Bax, that accelerates programmed cell death. *Cell* **74**, 609–619.

[36] Shan X, Fu YS, Aziz F, Wang XQ, Yan Q, and Liu JW (2014). Ginsenoside Rg3 inhibits melanoma cell proliferation through down-regulation of histone deacetylase 3 (HDAC3) and increase of p53 acetylation. *PLoS One* **9**, e115401.

[37] Zhou Y and Ho WS (2014). Combination of liquiritin, isoliquiritin and isoliquirigenin induce apoptotic cell death through upregulating p53 and p21 in the A549 non-small cell lung cancer cells. *Oncol Rep* **31**, 298–304.